12674–12688 *Nucleic Acids Research, 2022, Vol. 50, No. 22* *Published online 9 December 2022*
https://doi.org/10.1093/nar/gkac1144

PAM-independent ultra-specific activation of CRISPR-Cas12a via sticky-end dsDNA

Wei Zhang[1,2,†], Yaoqin Mu[1,†], Kejun Dong[2], Lei Zhang[1], Bei Yan[1], Hao Hu[1], Yangwei Liao[1], Rong Zhao[2], Wan Shu[2], Zhengxin Ye[1], Yaping Lu[3], Chong Wan[4], Qiangqiang Sun[5], Longjie Li[1,6,*], Hongbo Wang[2,*] and Xianjin Xiao[1,*]

[1]Institute of Reproductive Health, Tongji Medical College, Huazhong University of Science and Technology, Wuhan 430030, China, [2]Department of Obstetrics and Gynecology, Union Hospital, Tongji Medical College, Huazhong University of Science and Technology, Wuhan 430000, China, [3]Sinopharm Genomics Technology Co., Ltd, Wuhan 430000, China, [4]Precision Medicine Center, Yangtze Delta Region Institute of Tsinghua University, Jiaxing 314006, China, [5]Life Health Care Clinical Laboratories, Beijing 100000, China and [6]School of Life Science and Technology, Wuhan Polytechnic University, Wuhan 430023, China

Received September 25, 2022; Revised November 04, 2022; Editorial Decision November 08, 2022; Accepted November 18, 2022

ABSTRACT

Although CRISPR-Cas12a [clustered regularly interspaced short palindromic repeats (CRISPR)-CRISPR-associated protein 12a] combining pre-amplification technology has the advantage of high sensitivity in biosensing, its generality and specificity are insufficient, which greatly restrains its application range. Here, we discovered a new targeting substrate for LbaCas12a (Lachnospiraceae bacterium Cas12a), namely double-stranded DNA (dsDNA) with a sticky-end region (PAM$^-$SE$^+$ dsDNA). We discovered that CRISPR-Cas12a had special enzymatic properties for this substrate DNA, including the ability to recognize and cleave it without needing a protospacer adjacent motif (PAM) sequence and a high sensitivity to single-base mismatches in that substrate. Further mechanism studies revealed that guide RNA (gRNA) formed a triple-stranded flap structure with the substrate dsDNA. We also discovered the property of low-temperature activation of CRISPR-Cas12a and, by coupling with the unique DNA hybridization kinetics at low temperature, we constructed a complete workflow for low-abundance point mutation detection in real samples, which was fast, convenient and free of single-stranded DNA (ssDNA) transformation. The detection limits were 0.005–0.01% for synthesized strands and 0.01–0.05% for plasmid genomic DNA, and the mutation abundances provided by our system for 28 clinical samples were in accordance with next-generation sequencing results. We believe that our work not only reveals novel information about the target recognition mechanism of the CRISPR-Cas12a system, but also greatly broadens its application scenarios.

INTRODUCTION

The clustered regularly interspaced short palindromic repeats (CRISPR) system provides the prokaryotic adaptive immune system to bacteria to degrade intruding nucleic acids (1). Recently, because more and more scientists are keen to examine and study in depth the working mechanism of the CRISPR system, it has emerged as a groundbreaking tool for genome editing, transcriptional regulation and molecular diagnostics (2–4). CRISPR-associated protein 12a (Cas12a) and Cas9, as the two most influential and promising members, mediate crRNA-guided (gRNA) DNA cleavage by recognizing two key distinct sequence elements in the target double-stranded DNA (dsDNA) (5–7). These elements are (i) a 'protospacer' sequence, identified by Watson–Crick base-pairing interactions with gRNA and (ii) a protospacer adjacent motif (PAM), identified via sequence- and/or shape-specific protein–DNA interactions. CRISPR-Cas12a is distinct from CRISPR-Cas9 in that CRISPR-Cas12a uses a single CRISPR RNA as gRNA and can cleave single-stranded DNA (ssDNA) without requiring the PAM sequence (8,9). Moreover, the CRISPR-Cas12a system has the target loading-activated non-canonical *trans*-cleavage endonuclease activity toward ssDNA with very high turnovers (collateral effect) that makes it prominent in the fields of nucleic acid detection

*To whom correspondence should be addressed. Tel: +86 027 8369 2651; Fax: +86 027 8369 2651; Email: xiaoxianjin@hust.edu.cn
Correspondence may also be addressed to Hongbo Wang. Email: hb_wang1969@sina.com
Correspondence may also be addressed to Longjie Li. Email: lilongjie@whpu.edu.cn
†The authors wish it to be known that, in their opinion, the first two authors should be regarded as Joint First Authors.

and biosensing beyond its application in gene editing (9,10). At present, several CRISPR-based diagnostic technologies, such as DETECTR (10), HOLMES (11) and others (12–14), have been developed using different pre-amplification methods [recombinase polymerase amplification (RPA), loop-mediated isothermal amplification (LAMP) and polymerase chain reaction (PCR)] to reach an attomolar-level detection sensitivity.

The fundamental reason why CRISPR-Cas12a is prominent in the fields of nucleic acid detection and biosensing is that its *trans*-cleavage activity provides a new mode of signal amplification. It is established that the traditional signal amplification method combines the probe and target strand to generate a signal through nuclease digestion or an ingenious DNA reaction circuit, and then release the target strand to combine with the next probe to recycle the substrate strand and amplify its signal (15–18). In contrast, rather than amplifying the signal through the 'target strand cycle', CRISPR-Cas12a activates its *trans*-cleavage activity after binding of the Cas12a–gRNA complex with the target strand, thereby continuously cleaving the abundant fluorescent DNA probes in the solution to achieve signal amplification (10,11). Periodic DNA binding and dissociation processes are kinetically slow and thermodynamically subtle, and prone to insufficient signal intensity and significant background leakage (15). The CRISPR-Cas12a-mediated signal amplification process is completely separate from the probe/target binding process, which has the advantages of simplicity, rapidity and a high signal-to-noise ratio (19).

The powerful signal amplification ability of the CRISPR-Cas12a system leads to ultra-high sensitivity for target DNA recognition. However, in addition to sensitivity, specificity and generality are also very important for the CRISPR-Cas12a system (20,21). Sensitivity refers to the minimum number of targets that can be recognized. In real applications, the target DNA sequence may vary (22); thus, the capability of the CRISPR-Cas12a system should be generalized to any sequence of interest. Furthermore, the target DNA is not in isolation but rather immersed in a multitude of interfering sequences (23,24). Therefore, the characterization of the specificity (or targeting efficiency) of the system's ability is critical to discriminate between the target DNA and interfering sequences.

However, the working mechanism of CRISPR-Cas12a described above indicated that its generality is restricted to ssDNA, i.e. it requires a PAM to recognize the target dsDNA and not the target ssDNA (9,25). Consequently, in CRISPR-Cas12a-based detection systems, researchers usually need to set the target strand to be detected as ssDNA (13,26). If the target strand must be dsDNA, it needs to be made single-stranded by means such as enzyme digestion. This restrictive generality not only sacrifices the targeting range or procedural convenience, but also is additionally troublesome to CRISPR-Cas12a's specificity that is originally poor (27,28). Typically, an important criterion for evaluating the specificity of a detection system is its ability to discriminate between interfering strands with only a single base difference (29,30). Although CRISPR-Cas12a can recognize single-base mismatches in dsDNA by delicately adjusting the mismatch site within the seed domain, the DF (discrimination factor, which refers to the ability to distinguish target strands and interfering strands with only a single base difference) is not ideal; it is only 2- to 5-fold (11,28,31–33). Moreover, when CRISPR-Cas12a acted on ssDNA, its ability to discriminate single-base mismatches became much worse, close to zero (34). Even by introducing the commonly used method of adding a short competitive blocker strand (∼20 nt) to improve the specificity (35), the DFs were only marginally improved to 1.6- to 3.9-fold (Figure 1E). As we know, the detection of disease-related gene mutations has the greatest clinical significance and range of applications in the field of nucleic acid sensing (36,37). It is important to note that the ability of a detection method to distinguish single-base mismatch is critical for detecting point mutations associated with diseases, especially cancers (38–40). Moreover, in tumor liquid and early-stage tumor tissue biopsies, the abundance of mutations is very low (0.01–10%) (41–43). Therefore, this places a high demand on the ability of the detection system to discriminate between single-base mismatches. However, the ability of CRISPR-Cas12a to recognize single-base mismatches in dsDNA or ssDNA reported in previous studies does not yet meet the needs of clinical detection. Conclusively, CRISPR-Cas12a-based detection systems have high sensivity. However, their generality is limited to ssDNA and their specificity is very poor and far from meeting clinical requirements. Therefore, it is urgent to expand the generality and greatly improve the specificity of CRISPR-Cas12a system while maintaining its high sensitivity.

We believe the fundamental cause of the above difficulties is the limited types of substrate DNA for the CRISPR-Cas12a system and insufficient knowledge regarding the interactions between them. In this study, we thoroughly investigated the interaction between CRISPR-Cas12a and substrate DNA, and discovered a new targeting substrate for CRISPR-Cas12a, namely dsDNA with a sticky-end region. More importantly, we discovered that CRISPR-Cas12a had special enzymatic properties for this substrate DNA. These are (i) the ability to recognize and cleave dsDNA without needing a PAM sequence and (ii) a high sensitivity toward mismatches within the substrate, allowing for a significant improvement of the DF. Through in-depth mechanistic analysis, we found that the gRNA can form a triplex flap structure with the dsDNA containing a sticky-end region. This triplex flap structure not only guides CRISPR-Cas12a to cleave dsDNA without a PAM sequence, but is also more sensitive to mismatches. Based on the new target recognition features of CRISPR-Cas12a, we further introduced Helper strands that enabled the detection system to achieve a 154- to 1412- (median 200-) fold DF for target strands and interfering strands with a single-base difference, and a detection limit of low-abundance target strands of 0.01–0.05% in clinical samples. Furthermore, we discovered the 'low temperature activation phenomenon of the CRISPR-Cas12a system', and combined DNA hybridization kinetics and nucleic acid amplification techniques (conventional PCR or isothermal amplification techniques such as RPA) to construct a rapid and simple mutation detection technology that did not need to handle the amplification product. This technology demonstrated a robust detection performance for both genomic DNA and clinical

samples. In summary, we discovered a new targeting substrate for CRISPR-Cas12a on which the sensitivity, specificity (discrimination toward a single-base difference) and universality (PAM independent) achieved a high degree of connectivity. The additional discovery of the 'low temperature activation phenomenon' enables the CRISPR-Cas12a system to be easily combined with nucleic acid amplification technology to achieve fast, simple, accurate and highly sensitive mutation detection.

MATERIALS AND METHODS

Time-based fluorescence acquisition

Time-based fluorescence data were acquired using Synergy HTX Multi-Mode Microplate Readers. We set the excitation wavelength at 485 nm and emission wavelength at 528 nm for FAM. Fluorescence intensity was recorded once a cycle (60 s per cycle) with a gain level of 90 at 37°C. The duration of fluorescence acquisition varies. Typically, we set a maximum acquisition duration of 4 h, but terminate the experiment early if it appears that the reaction has roughly reached equilibrium (in order to facilitate more rapid collection of data).

Design of primers and gRNAs

The principle of designing RPA primers is referred to in the TwistAmp Assay Design Manual (https://www.twistdx.co.uk/en/support/manuals/twistamp-manuals). Primers for PCR were designed using online tools of the NCBI (https://www.ncbi.nlm.nih.gov/).

Sequences used

gRNA strands were synthesized and purified by high-performance liquid chromatography (HPLC; Suzhou Genepharma). DNA strands were also synthesized and purified by HPLC (Sangon Co., China). The sequences of all the probes and DNA/RNA used in this work are summarized in Supplementary Tables S1–S7. DNase/RNase-free deionized water was purchased from Tiangen Biotech Co. (China).

CRISPR-Cas12a-FQ-reporter assay

Firstly, 1 μM LbaCas12a (Lachnospiraceae bacterium Cas12a protein; New England Biolabs), 0.5 μM gRNA were incubated in the 1× NEBuffer2.1 (New England Biolabs) buffer at 37°C for 30 min. To prepare the target stands, we mixed the B-stand and T-stand at a 1:2 or 1:5 ratio in 1× ThermoPol reaction buffer (New England Biolabs). The mixtures were then thermally annealed using a PCR machine, following a thermal profile of initial heating to 95°C for 5 min, and subsequent cooling to 50°C for 10 min, and then at 37°C for 60 min. To a 400 μl ELISA (enzyme-linked immunosorbent assay) plate, 100 or 200 nM target DNA strand, 20 nM LbaCas12a, 10 nM gRNA, 200 nM of ssDNA FQ probe (Sangon Co., China), 7.5 μl NEBuffer2.1 (10×) and 4 mM Mg^{2+} were added and brought up to a total volume of 50 μl by deionized water.

Construction and characterization of the AuNP–DNA probes

Gold nanoparticles (AuNPs; 20 nm diameter) and the FAM-labeled substrate strand were mixed at a molar ratio of 1:2000. The AuNP–DNA probes were constructed according to a previously reported study. Finally, the prepared AuNP–DNA probes were stored in 25 mM Tris–HCl (pH 7.4) at a concentration of 4 nM and kept at 4°C until use. Transmission electron microscopy (TEM; JEM-1400Flash, JEOL, Japan), Nanodrop2000 (Thermo, Germany) and Zetasizer Nano (Malvern, China) were used to characterize the bare AuNPs and AuNP–DNA probes.

Denaturing polyacrylamide gel electrophoresis (PAGE) experiment

For the polyacrylamide gel experiment, lanes 1–4 from left to right were loaded with 500 nM G1-B-10 strand and 500 nM G1-SE^{+}-T-19 strand, 750 nM LbaCas12a and 500 nM gRNA (lane 1); 500 nM G1-B-11 strand and 500 nM G1-SE^{+}-T-20 strand (lane 2); 500 nM G1-B-11 strand and 500 nM G1-SE^{+}-T-19 strand (lane 3); and 500 nM G1-B-10 strand and 500 nM G1-SE^{+}-T-19 strand (lane 4). To a 200 μl PCR tube, the above mix, 7.5 μl NEBuffer2.1 (10×) and 4 mM Mg^{2+} were added and brought up to a total volume of 50 μl by deionized water. The reaction process was 1 h, followed by 95°C for 30 min, 55°C for 5 min and then 37°C for 10 min. Then, DNA loading buffer (6×) (Sangon Co., China) was added to the tube. A 15% denatured polyacrylamide gel was used to separate the DNA strands. Electrophoresis was carried out at 100 V for 2 h. The gel was then removed and soaked in the dye solution (4S Red Plus Nucleic Acid Stain, Sangon Co.) for 30 min. The gel image was taken by Bio-rad ChemDoc XRS (Bio-Rad, USA).

RPA or PCR amplification

RPA was performed according to the TwistAmp Liquid Basic Quick Guide. Briefly, a 50 μl reaction mixture including 2 μl of DNA sample, 29.5 μl of Rehydration buffer, 2.4 μl of RPA-F/R solution (forward primer, reverse primer, 10 μM), 2.5 μl of magnesium acetate (280 mM) and 11.2 μl of ddH_2O was incubated at 37°C for 20 min. For PCR amplification: in a 200 μl PCR tube, 2 μl of 10× ThermolPol Reaction Buffer, 2 μl of dNTPs (10 nmol), 1 μl of forward primer (5 μM), 1 μl of reverse primer (5 μM), 20 ng of genomic DNA templates and 0.4 U of Taq DNA polymerase were added and the total volume was brought up to 25 μl by deionized water. The PCR procedure (95°C for 15 s, 60°C for 30 s, 72°C for 15 s, 40 cycles) was performed on a StepOne Plus Real-Time PCR System (Applied Biosystems, USA). Then, the RPA or PCR was added for CRISPR-Cas12a cleavage assay.

Human clinical sample collection and preparation

The human clinical sample was from the precision medicine center, Yangtze Delta region institute of Tsinghua University, Jiaxing. It has been reviewed and approved by the Medical Ethics Committee of Tongji Medical College of Huazhong University of Science and Technology, and the project number is [2022] IEC (A131). The human genomic

DNA was extracted from blood using the Tiangen Kit (China) and determined by Nanodrop2000 (Thermo, Germany). The analyte genomic DNA diluted to a concentration of 100 ng/μl, and 2 μl of the diluted sample was added into the RPA tube to achieve a final concentration of 4 ng/μl (50 μl).

Detection of low abundance mutations in plasmid or human genomic DNA

After RPA or PCR amplification, the products were purified to obtain the target strands using a DNA Purification Kit (Tiangen Biotech Co.). The concentration of the purified products were measured by Nanodrop2000. Then, Helper strand with 10-fold amount over target strand was added. The mixtures were thermally annealed using a PCR machine, following a thermal profile of initial heating to 95 °C for 10 min, subsequent cooling to 0 °C for 5 min and then adding CRISPR-Cas12a mix at 0°C for 10 min. The solutions were immediately put into a Synergy HTX Instrument for fluorescence measurement. Fluorescence intensity was recorded once a cycle (60 s per cycle) with a gain level of 90 at 37°C.

Statistical analysis

GraphPad Prism version 8 was used for all statistical analyses. Data are presented as the mean ± standard deviation (SD). Student's *t*-tests and one-way analysis of variance (ANOVA) were used for two group and multigroup comparisons, respectively. Differences were considered statistically significant at $P < 0.05$, $n = 3$.

RESULTS AND DISCUSSION

The enzymatic properties of CRISPR-Cas12a targeting sticky-end dsDNA

We first briefly inspected the recognition of conventional target strands by the CRISPR-Cas12a system. As shown in Figure 1A, we randomly designed gRNA-1, two classical substrates (10 nt blunt-end dsDNA with PAM and ssDNA, denoted as G1-B-1 and G1-PAM$^+$-T-1 respectively) and a derivative mode of the ssDNA classical substrate, i.e. ssDNA combined with a competitive blocker strand (ssDNA/blocker, G1-B-1/G1-Blocker-1). We then activated CRISPR-Cas12a using the classical substrate DNA described above and assessed the extent of activation by the rate at which activated CRISPR-Cas12a cleaved unrelated ssDNA probes. As expected, CRISPR-Cas12a showed very high catalytic efficiencies toward all classical substrates (Figure 1B). However, its specificity toward these substrates was very poor. We used randomly designed gRNA-1, gRNA-2 and gRNA-3 as our models. For each gRNA, we synthesized one targeting substrate DNA and six interfering substrate DNAs with a single base difference (G1-B-1 to -7, G2-B-1 to -7, G3-B-1 to -7 and the corresponding T-strands and blockers). As shown in Supplementary Figure S1a, the gRNA formed single-base mismatches with the B-strand of the interfering substrate DNAs at locations numbered as 1, 3, 6, 9, 12 and 15. Thereafter, we treated the aforementioned fluorescent CRISPR-Cas12a system with the above substrate DNAs. The experimental results showed that the DFs, defined as the ratio of the rate of increase of fluorescence intensity of the targeting DNA over that of the interfering DNA, were in the range of only 1.1–2.4 (median 1.38), indicating an extremely poor specificity (Figure 1C). The outcome was slightly better for PAM$^+$ dsDNA and ssDNA/blocker substrate, with DFs in the range of 1.4–4.3 (Figure 1D, median 2.46) and 1.6–3.9 (Figure 1E; Supplementary Figure S1b, median 2.3), respectively. Overall, the specificity of CRISPR-Cas12a toward the classical substrates (PAM$^+$ dsDNA, ssDNA and ssDNA/blocker) was very poor and far below clinical requirements.

As discussed in the Introduction, we believe the solution to the above problem lies in discovering novel recognition behavior of CRISPR-Cas12a. Fortunately, we discovered a novel substrate for CRISPR-Cas12a, namely sticky-end dsDNA. As shown in Figure 1F, the sticky-end region of the dsDNA (G1-B-1/G1-SE+-T-1) was a prolonged overhang within which we designed an initiation region that was complementary to the short domain of gRNA, and thereby initiated gRNA to further invade the substrate dsDNA. After invasion, the gRNA formed a triplex flap structure with the substrate DNA that activated the Cas12a and subsequently cleaved at both strands. The experimental results in Figure 1B showed that the sticky-end dsDNA, containing an initiation region without a PAM sequence (denoted as PAM$^-$SE$^+$ dsDNA), successfully activated the CRISPR-Cas12a as expected. In addition, the cleavage reaction reached a plateau within 10 min, indicating that the recognition efficiency of CRISPR-Cas12a for PAM$^-$SE$^+$ dsDNA was comparable with that of the classic substrate. We then further investigated the influence of the initiation region length on the recognition efficiency. As shown in Figure 1G, the results indicated that the recognition efficiency gradually increased with the enlargement of the initiation region, up to 5 nt, where the efficiency reached saturation (closer to the recognition efficiency of classical substrates, G1-SE$^+$-T-1 to 7). Notably, the substrate dsDNA was quite long; therefore, the gRNA was unable to displace the shorter strand of dsDNA, indicating that CRISPR-Cas12a did not recognize the PAM$^-$SE$^+$ dsDNA through the derivative mode of ssDNA, but recognized it as a real double-stranded substrate. Thereafter, we further investigated the recognition generality of CRISPR-Cas12a toward different PAM$^-$SE$^+$ dsDNAs. As shown in Figure 1H, CRISPR-Cas12a successfully recognized all seven randomly designed PAM$^-$SE$^+$ dsDNAs (gRNA-1 to -7 and the corresponding B- and T-strands), and the reaction rates were all reasonably fast. Based on the above data, we concluded that we had found a novel type of substrate DNA for CRISPR-Cas12a and discovered the unique PAM-independence property of CRISPR-Cas12a toward the novel substrate. This novel structure and unique property broadened the sequence generality of CRISPR-Cas12a from isolated ssDNA to partial dsDNA, which is extremely beneficial to the understanding and application of the CRISPR-Cas12a system.

As we discussed in the Introduction, apart from sequence generality, specificity is also vital for CRISPR-Cas12a. Surprisingly, and fortunately, we found that the novel struc-

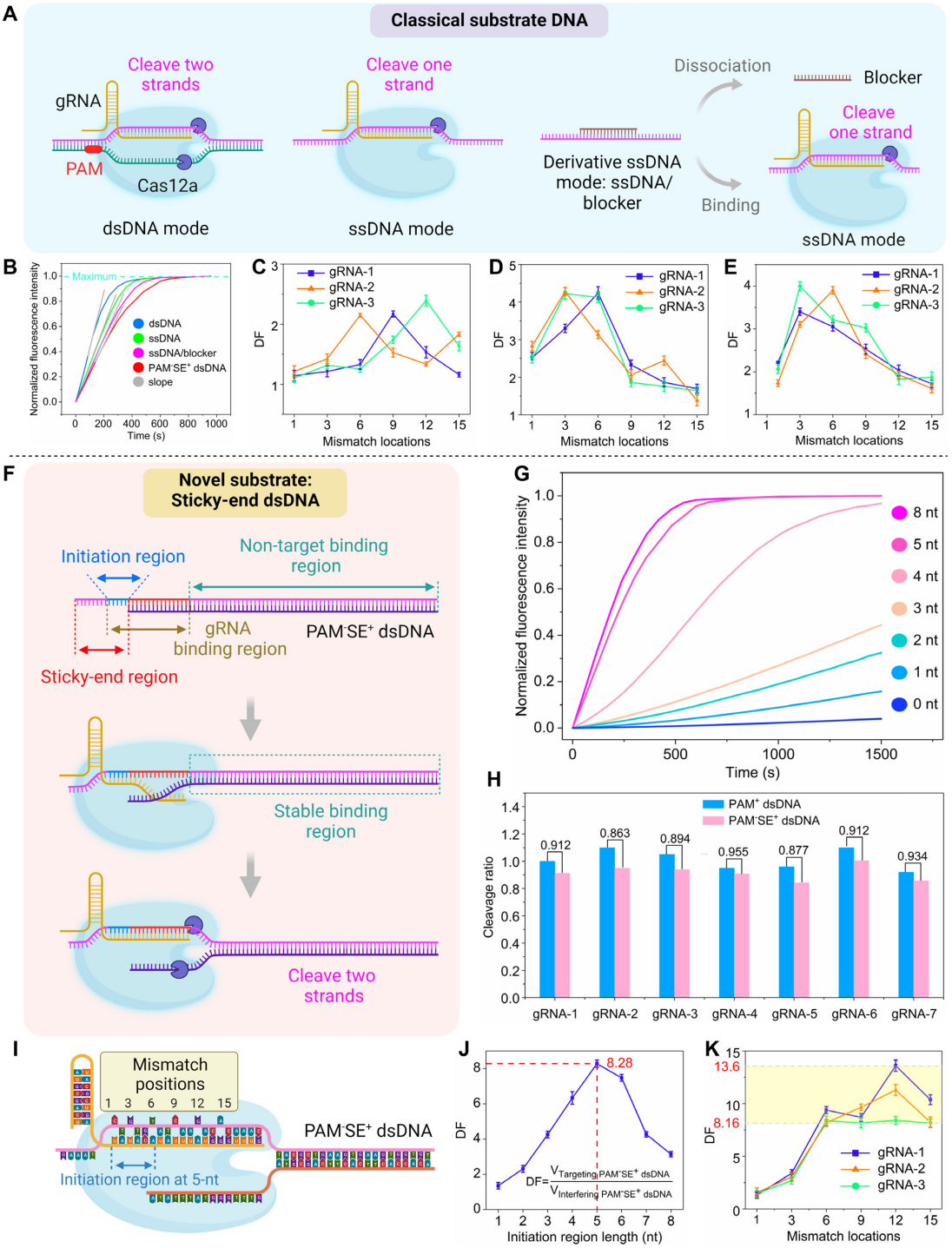

Figure 1. (**A**) Schematic illustration of CRISPR-Cas12a activated by three classical substrate DNAs: dsDNA with a PAM; ssDNA; and ssDNA/blocker. (**B**) The cleavage efficiency of CRISPR-Cas12a activated by dsDNA, ssDNA, ssDNA/blocker and dsDNA with a sticky-end region. (**C**) The DFs of the CRISPR-Cas12a system toward targeting ssDNA and interfering ssDNA with a single-base difference. (**D**) The DFs of the CRISPR-Cas12a system toward targeting dsDNA and interfering dsDNA with a single-base difference. (**E**) The DFs of the CRISPR-Cas12a system toward targeting ssDNA/blocker duplex and interfering ssDNA/blocker duplex with a single-base difference. (**F**) Schematic illustration of CRISPR-Cas12a activated by sticky-end long dsDNA. (**G**) The influence of the length of the initiation region on the cleavage efficiency of CRISPR-Cas12a toward PAM^{-}SE^{+} dsDNA. (**H**) The cleavage efficiency of CRISPR-Cas12a activated by seven randomly designed PAM^{-}SE^{+5} dsDNAs. (**I**) Schematic illustration of the positions of the mismatched site between gRNA and PAM-SE^{+5} dsDNA. The positions were numbered sequentially from the first nucleotide of gRNA within the hybridization domain. The initiation region was fixed at 5 nt. (**J**) The influence of the length of the initiation region on the DF of the CRISPR-Cas12a system toward targeting PAM^{-}SE^{+5} dsDNA and interfering PAM^{-}SE^{+5} dsDNA when mismatch located at position 9. (**K**) The DFs of the CRISPR-Cas12a system toward targeting PAM^{-}SE^{+5} dsDNA and different interfering PAM^{-}SE^{+5} dsDNAs with the mismatches located at positions 1, 3, 6, 9, 12 and15. Three randomly designed gRNAs were tested, and the initiation regions were fixed at 5 nt. In all the above experiments, reaction settings are as follows: 200 nM B-strand, 400 nM T-strand or blocker strands, 20 nM LbaCas12a, 10 nM gRNA and 200 nM ssDNA FQ probe (labeled with FAM and BHQ-1).

ture also enhanced the specificity of CRISPR-Cas12a. We first showed that the specificity of CRISPR-Cas12a toward classical substrates, including ssDNA, dsDNA and ssDNA/blocker, was very poor (Figure 1C, 1AD and 1AE). To solve this problem, we thoroughly investigated the specificity of CRISPR-Cas12a toward the novel PAM$^-$SE$^+$ dsDNA. Using gRNA-1 as the model, we synthesized eight sets of PAM$^-$SE$^+$ dsDNAs with the initiation length ranging from 1 to 8 nt (G1-SE$^+$-T-8 to -15). For each set of PAM$^-$SE$^+$ dsDNA, we designed a targeting and a single-base difference interfering type that formed a mismatch with gRNA-1 at location 9 (Supplementary Figure S1c). As shown in Figure 1J, CRISPR-Cas12a showed higher specificity toward PAM$^-$SE$^+$ dsDNAs than classical substrates when the length of the initiation region was in the range of 3–7 nt, and the DF reached a maximum of 8.28 when PAM$^-$SE^{+5} dsDNA was tested. We then fixed the initiation length at 5 nt and adjusted the mismatch locations from 1 to 15 (Figure 1I, G1-B-2–7, G1-SE$^+$-T-6, 12, 15–17). Experimental results in Figure 1K showed that the CRISPR-Cas12a had little discrimination ability toward mismatches located within the initiation domain (locations 1 and 3), but its specificity increased dramatically to 8.2–11.3 (median 8.6) for mismatches located within the branch migration domain (locations 6, 9, 12 and 15), nearly 4-fold higher than for classical substrates. The above phenomenon was also observed when using gRNA-2 and gRNA-3 (Figure 1K, G2-B-2 to -7, G3-B-2 to -7 and the corresponding G-SE$^+$-T). Overall, we have revealed that the CRISPR-Cas12a was very sensitive to mismatches within the branch migration domain of PAM$^-$SE^{+5} dsDNAs and showed 4-fold higher specificity over classical substrates.

Hyperdiscrimination toward single-base mismatches via a two mismatches versus one mismatch strategy

Although the specificity of CRISPR-Cas12a had been increased by 4-fold between 8.2 and 11.3, this was still insufficient as the detection limit for low-abundance targeting strands was only in the range of 5–10% (Supplementary Figure S2a, b). To further enhance the specificity of CRISPR-Cas12a, we artificially altered one base of gRNA so that it would form one single-base mismatch with the targeting PAM$^-$SE^{+5} dsDNA and two consecutive single-base mismatches with the interfering PAM$^-$SE^{+5} dsDNA (Figure 2A, B). According to previous literature,

artificial mismatches located around the targeting mismatch site make a larger difference to the local environment of the reaction center and might inhibit the undesired signal better (10). Therefore, for all the targeting mutations, we evaluated the enhancement of specificity produced by artificial mismatch next to or 2 nt away from the targeting mismatch, and we found that there was no empirical rule. We then chose the optimal location of an artificial mismatch for each targeting mutation to conduct subsequent experiments. In detail, we synthesized 12 sets of PAM$^-$SE^{+5} dsDNAs (G1-B-4 to -7, G2-B-4 to -7, G3-B-4 to -7 and the corresponding G-SE$^+$-T) and, for each set, there was one targeting dsDNA and one interfering dsDNA with a single-base difference. According to the location of the interfering base, the above 12 sets of dsDNAs could be evenly distributed into four groups, with the interfering base located at 6, 9, 12 and 15. We then synthesized the corresponding gRNAs (gRNA-8 to -19) for each set and investigated the specificity of CRISPR-Cas12a for this new scenario. As shown in Figure 2C, the DFs increased significantly, reaching 30.9–631.5 (median 44), and the detection limit for the low-abundance targeting strand decreased to the range of 0.5–0.1% (Figure 2D; Supplementary Figure S2c). In contrast, if we adopt the above 'two mismatches versus one mismatch' strategy for classical PAM$^+$ dsDNA, the DFs could only be elevated to 4.9–50 (Supplementary Figure S2d, median 11.5, G1-B-4 to -7, G2-B-4 to -7, G3-B-4 to -7 and the corresponding G-PAM$^+$-T), which further demonstrated that CRISPR-Cas12a was more sensitive to the sequence alterations which occurred in PAM$^-$SE^{+5} dsDNAs.

Mechanism of CRISPR-Cas12a targeting sticky-end dsDNA

We next delved into the catalytic process to uncover the underlying mechanism of CRISPR-Cas12a recognizing PAM$^-$SE^{+5} dsDNAs. Using gRNA-1 as the model, we synthesized its targeting PAM$^-$SE^{+5} dsDNA (G1-B-9, G1-SE$^+$-T-19), within which the T-strand was labeled with a fluorophore (FAM) at its 5' end and a quencher (BHQ-1) at the 16th nucleotide from the 5' end. As shown in Figure 3A, 200 nM of free T-strand, which was randomly coiled in the solution, emitted a fluorescence intensity of ∼38 000 (curve a). When the T-strand hybridized to the B-strand, the randomly coiled structure was stretched and the fluorescence intensity increased to ∼190 000 (curve b). Should the T-strand cleave, the FAM would completely tear away from the quencher, increasing the fluorescence intensity to ∼300 000 (curve c). We then treated the FAM-labeled PAM$^-$SE^{+5} dsDNA with the CRISPR-Cas12a system and observed the fluorescence intensity initially decrease from 180 000 to 9700 and then increase to 295 000 until it plateaued, as shown in Figure 3A. This 'down and up' pattern was also observed in the FAM-labeled PAM$^-$SE^{+5} dsDNA (Supplementary Figure S3, G2-B-8/G2-SE$^+$-T-6). After carefully analyzing the catalytic process, we attributed the initial decrease in fluorescence to the formation of a triplex flap structure between gRNA and PAM$^-$SE^{+5} dsDNA. The flap structure was induced by the gRNA and T-strand branch migrating on the B-strand. The flapped T-strand was less stretched and closer to the quencher, resulting in the decrease in fluorescence intensity. The triplex

flap structure activated Cas12a, and the subsequent increase in fluorescence intensity indicated that the activated Cas12a cleaved both strands of the substrate dsDNA rather than the B-strand alone. To further demonstrate that the cleavage occurred on both strands in a more straightforward way, we relocated the labeling sites. As shown in Figure 3B and C, we designed two sets of B-strand/T-strand (G1-SE$^+$-T-20, G1-SE$^+$-T-21). In Figure 3B, FAM and BHQ-1 were both labeled on the T-strand but with a much closer distance of only 8 nt. In Figure 3C, BHQ-1 and FAM were labeled on the B- and T-strands, respectively. The experimental results indicated that subsequent to addition of the CRISPR-Cas12a system, the fluorescent signal con-

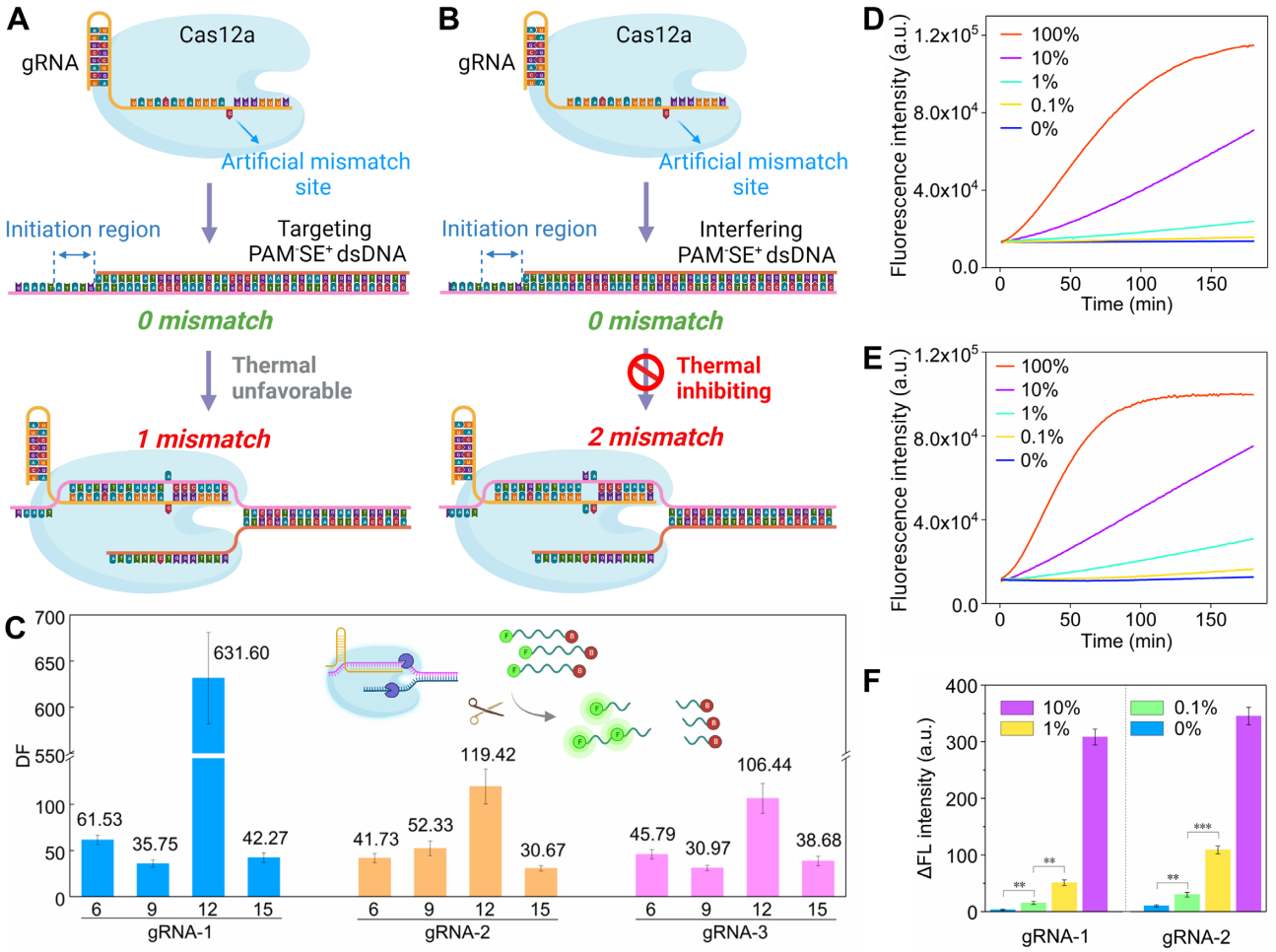

Figure 2. (**A**) and (**B**) Schematic illustration of the design of an artificial mismatch between gRNA and PAM$^-$SE^{+5} dsDNA to enhance the specificity of the CRISPR-Cas12a system toward targeting and interfering PAM$^-$SE^{+5} dsDNA with a single-base difference. (**C**) The DFs of the CRISPR-Cas12a system toward targeting PAM$^-$SE^{+5} dsDNA and interfering PAM$^-$SE^{+5} dsDNAs with a single-base difference when the non-artificial mismatch was located at positions 6, 9, 12 and 15. Three randomly designed gRNAs were tested. Reaction setup: 100 nM B-strands, 200 nM T-strand, 20 nM LbaCas12a, 10 nM gRNA and 200 nM ssDNA FQ probe. (**D–F**) Detection of low-abundance targeting PAM$^-$SE^{+5} dsDNA. gRNA-1 (D) and gRNA-2 (E) were used. the non-artificial mismatch located at position 12. Reaction setup: 200 nM B-strand, 400 nM T-strand, 20 nM LbaCas12a, 10 nM gRNA and 200 nM ssDNA FQ probe. All the above experiments were conducted in triplicate. Results are shown as the mean ± SD. Student's *t*-test, ns, $P > 0.05$; *$P < 0.05$; **$P < 0.01$; ***$P < 0.001$.

tinued to increase until a plateau, close to the signal of positive control, was reached (FAM-labeled T-strand), demonstrating that CRISPR-Cas12a cleaved the flapped T-strand. The denatured polyacrylamide gel experiment results in Figure 3D also confirmed our speculation (G1-B-10, G1-B-11, G1-SE$^+$-T-19 and G1-SE$^+$-T-20). The cleaved products in lane 1 aligned exactly with lane 2 which corresponded to the products of Cas12a cleaving classical PAM$^+$ dsDNA. Therefore, we have firmly demonstrated that CRISPR-Cas12a recognized sticky-end dsDNA as 'real' dsDNA and cleaved it on both strands. The cleavage sites on sticky-end dsDNA were exactly the same as those on conventional PAM-containing dsDNA. Based on the catalytic mechanism, we could further explain the exceptional specificity of CRISPR-Cas12a toward PAM$^-$SE^{+5} dsDNA. As shown in Figure 3E, CRISPR-Cas12a not only discriminated mismatches within the initiation domain but presented exceptional specificity toward mismatches within the branch migration domain. The above phenomenon indicates that the system's specificity originated from the triplex flap structure. The flapping between the gRNA and T-strand was thermodynamically balanced ($\Delta G \approx 0$) and therefore very sensitive to sequence alterations; even slight changes had the ability to cause considerable unbalanced flapping and such unbalanced flapping could be sensitively recognized by CRISPR-Cas12a.

In conclusion, we thoroughly investigated the recognition behavior of CRISPR-Cas12a toward classical substrates and the newly discovered non-classical substrate, and demonstrated that CRISPR-Cas12a could not only efficiently recognize initiation region-containing dsDNA without a PAM sequence but also showed exceptional specificity toward sequence alterations occurring in the branch migration domain of PAM$^-$SE^{+5} dsDNAs. The specificity could be 30.9–631.5 (median 44), which was nearly 4-fold higher than classical substrates. A further mechanistic study revealed that gRNA and PAM$^-$SE^{+5} dsDNAs would form a triplex flap structure and subsequently activated

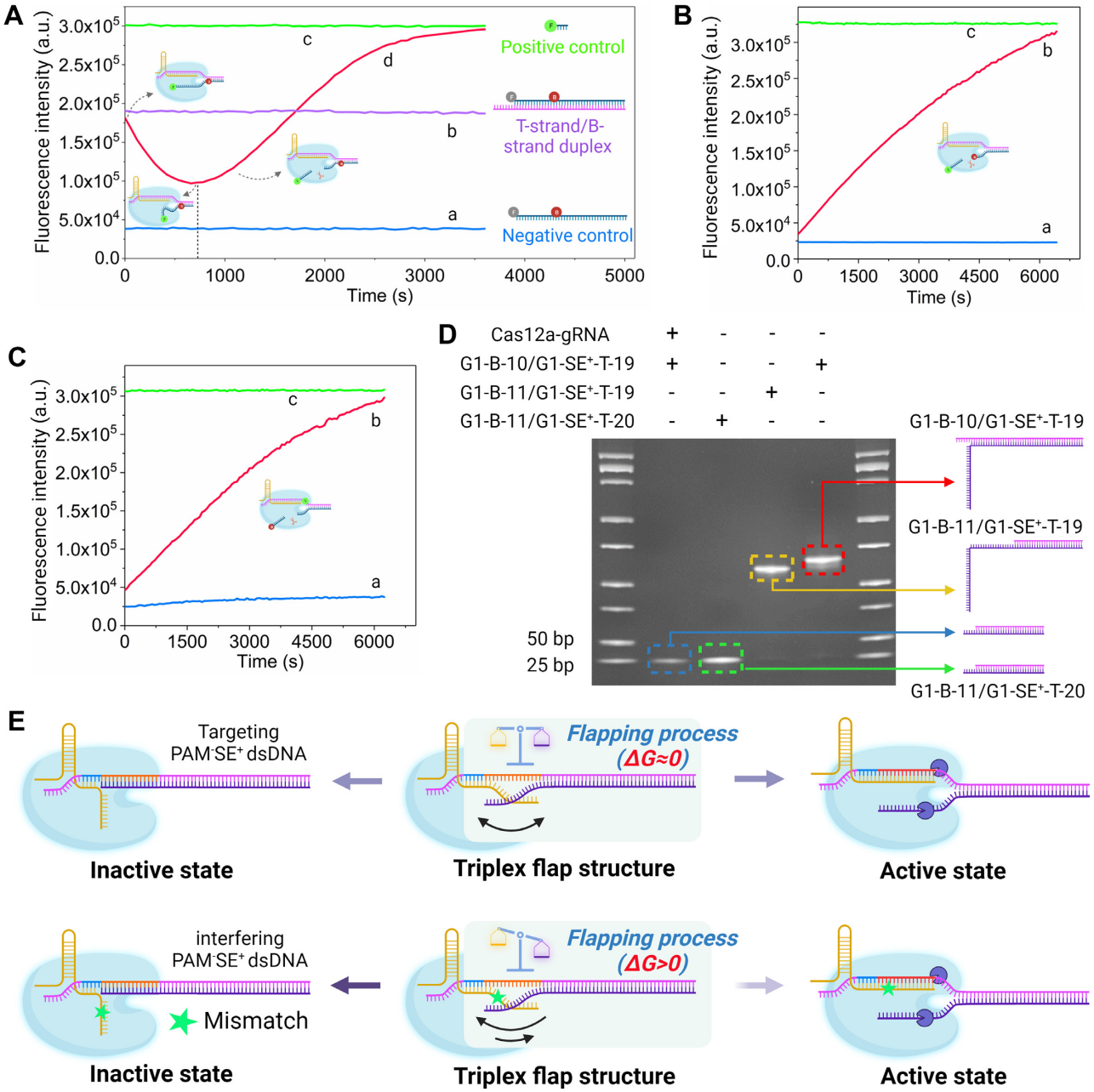

Figure 3. (**A**) The CRISPR-Cas12a system activated by the PAM^{-}SE^{+5} dsDNA in which the T-strand was labeled with a FAM at its 5' end and a BHQ-1 at the 16th nucleotide from the 5' end. Curve a: negative control; curve b: the T-strand/B-strand duplex; curve c: positive control; curve d: experimental group. The reaction system comprised 200 nM B-strand, 200 nM T-strand (labeled with FAM and BHQ-1), 400 nM LbaCas12a and 200 nM gRNA; positive control: 200 nM FAM-labeled ssDNA; negative control: 200 nM T-strand (labeled with FAM and BHQ-1). (**B**) The CRISPR-Cas12a system activated by the PAM^{-}SE^{+5} dsDNA in which the FAM and BHQ-1 labeled on the T-strand were much closer (8 nt, curve b). The negative control (curve a) and positive control (curve c) were the same a those in (A). Reaction setups were also the same as in (A). (**C**) The CRISPR-Cas12a system activated by the PAM^{-}SE^{+5} dsDNA in which the B-strand and T-strand were labeled with BHQ-1 and FAM, respectively (curve b). The negative control (curve a) and positive control (curve c) were the same as those in (A). The reaction system comprised 200 nM B-strand (labeled with BHQ-1), 200 nM T-strand (labeled with FAM), 400 nM LbaCas12a and 200 nM gRNA; positive control: 200 nM FAM-labeled ssDNA; negative control: 200 nM B-strand (labeled with BHQ-1) and 200 nM T-strand (labeled with BHQ-1). (**D**) Characterization of the products of CRISPR-Cas12a cleaving PAM^{-}SE^{+5} dsDNAs by denaturing PAGE. Lanes 1–4 from left to right: lane 1, 500 nM G1-B-10 strand, 500 nM G1-SE^{+}-T-19 strand, 750 nM LbaCas12a and 500 nM gRNA; lane 2, 500 nM G1-B-11 strand and 500 nM G1-SE^{+}-T-20 strand; lane 3, 500 nM G1-B-11 strand and 500 nM G1-SE^{+}-T-19 strand; lane 4, 500 nM G1-B-10 strand and 500 nM G1-SE^{+}-T-19 strand. (**E**) The assumed mechanism of the exceptional specificity of CRISPR-Cas12a toward PAM^{-}SE^{+5} dsDNA: the triplex flap structure between the gRNA and T-strand. The length and the depth of color of the arrow indicate the tendency of the reaction.

CRISPR-Cas12a to cleave both strands of the dsDNA. Importantly, CRISPR-Cas12a was very sensitive to sequence alterations in the triplex flap structure, leading to its exceptional specificity. Compared with previously reported examples of PAM-less dsDNA activating CRIPSR-Cas12a, such as the bubble-containing dsDNA (44) and the derivative ssDNA mode depicted in Figure 1A, our strategy possessed unique advantages. Although the substrate in the derivative ssDNA mode 'seemed' to be dsDNA, the 'real' substrate was actually the residual ssDNA after the shorter strand of the targeting dsDNA had been displaced by gRNA. Therefore, the derivative ssDNA mode cannot be recognized as a PAM-less dsDNA activation strategy. As for the bubble-containing dsDNA, our proposed sticky-end dsDNA was more natural, or at least much easier to prepare, so our findings were compatible with a wider range of applications. More importantly, using sticky-end dsDNA, we could solve the bottleneck problem of poor specificity of Cas12a and unleash its great potential in detecting low-abundance point mutations.

Detection of low-abundance point mutations by introducing the Helper strand

Based on our findings, we then endeavored to exploit the CRISPR-Cas12a system for further applications in molecular diagnosis of low-abundance point mutations. Taking advantages of all the properties found in our experiments, we came up with a promising detection mode as shown in Figure 4A and B: setting ssDNA as the target and introducing a Helper strand. The Helper strand was designed to be complementary to the wild-type ssDNA (WT) and single-base mismatched with the mutant type ssDNA (MT) at locations 6 or 12 (G1-Helper-1–2, G2-Helper-1–2, G3-Helper-1–2 and the corresponding gRNA and G-B strands). The sequence and length of the Helper strand were intentionally adjusted to form $PAM^{-}SE^{+5}$ dsDNA with MT or WT. We then could adopt the 'two mismatches versus one mismatch' strategy, in which the gRNA

formed two mismatches with the WT and only one mismatch with the MT. According to the aforementioned results, the CRISPR-Cas12a system couldhardly recognized the WT/Helper duplex, similarly to the recognition of interfering $PAM^{-}SE^{+5}$ dsDNA of Figure 2B. In contrast, we assumed that the CRISPR-Cas12a would not only recognize the MT/Helper duplex efficiently, but that this would be even better than its recognition of the targeting $PAM^{-}SE^{+5}$ dsDNA of Figure 2A, as the MT/Helper duplex was mismatched, which was easier for the invasion of gRNA and formation of the triplex flap structure. The experimental results shown in Figure 4C and D and Supplementary Figure S4a demonstrated our assumption: the DFs increased to 155–1411 (median 207) and the detection limit for the low-abundance targeting strand reached as low as 0.0005%. To the best of our knowledge, this is an ultra-high level of specificity and functionality that is far beyond the reach of current CRISPR-Cas12a-based assays.

All the above experiments were conducted on random strands without clinical relevance. To further evaluate the generality and clinical potential of our method, we applied the system to six point mutations with definite clinical significance, namely EGFR T790M, EGFR S768I, TP53 R248W, PARP1/T>G (location of the mutated nucleotide in chromosome: 226553653, sequencing information was provided by the Sinopharm Genomics Technology Co.), BRAF V600E and PIK3CA E545D. We synthesized the corresponding gRNA, MT, WT and Helper strands (DNA sequences are given in Supplementary Table S4). As shown in Figure 4E, the DFs toward the tested mutations ranged from 154 to 446 (median 207), and the detection limit for low-abundance point mutations reached 0.005–0.01% (Figure 4F, G; Supplementary Figure S4b–f). The performance matched the results of the aforementioned random strands, demonstrating the generality and clinical potential of our proposed system.

Low-temperature activation of CRISPR-Cas12a and workflow for low-abundance mutation detection on genomic DNA

In clinical practice, the CRISPR-Cas12a system is usually coupled with the preceding PCR amplification process. As we know, the PCR products, no matter whether using conventional thermal PCR or the later developed isothermal PCR, were all blunt-end dsDNA. Therefore, to be compatible with the 'Helper mode' of our established system, the blunt-end dsDNA product needs to be transformed to ssDNA, which is a complicated and erratic process. A convenient and robust method for transforming dsDNA to ssDNA has long been a key demand in the field of mutation detection, especially for post-PCR methods. Herein, we have found another novel property of CRIPSR-Cas12a: recognition and activation at low temperature (∼0°C) and, combined with the unique DNA hybridization kinetics during the process of denaturation and rapid annealing, we have developed a very convenient transformation strategy for the CRISPR-Cas12a system. The workflow (numbered as workflow 1) is illustrated in Figure 5A. After conventional thermal PCR or isothermal RPA, the 94–117 bp double-stranded PCR products and a 10-fold excess of the 36–40 nt Helper strand were heated to 95°C for 10 min. Then, the reaction tube was immediately put on ice and incubated for 5 min. During this step, the double strands of PCR products would not hybridize due to the slow kinetics at 0°C, whereas the Helper strand was able to hybridize with targeting strand owing to its high concentration. Next, the CRISPR-Cas12a system was added and incubated on ice for 10 min. Finally, the fluorescent single-stranded probe was added and the reaction system was immediately put into a microplate reader for fluorescence measurement at 37°C. We then took EGFR T790M as our targeting mutation, and synthesized mutant-type and wild-type plasmids and primers (EGFR-T790M-MT-L, EGFR-T790M-WT-L, EGFR-T790M-Helper and RPA-FP/RP-1). After RPA, the above workflow was adopted and, as shown in Figure 5F, the mutant-type plasmid produced a strong fluorescent signal and the DF reached 257, demonstrating that our established CRISPR-Cas12a system was compatible with PCR amplification by performing a simple heating and annealing procedure. We then further investigated the function of the heating and annealing procedure. As illustrated in Figure 5B and C, we designed two other workflows: for workflow 2, the PCR products

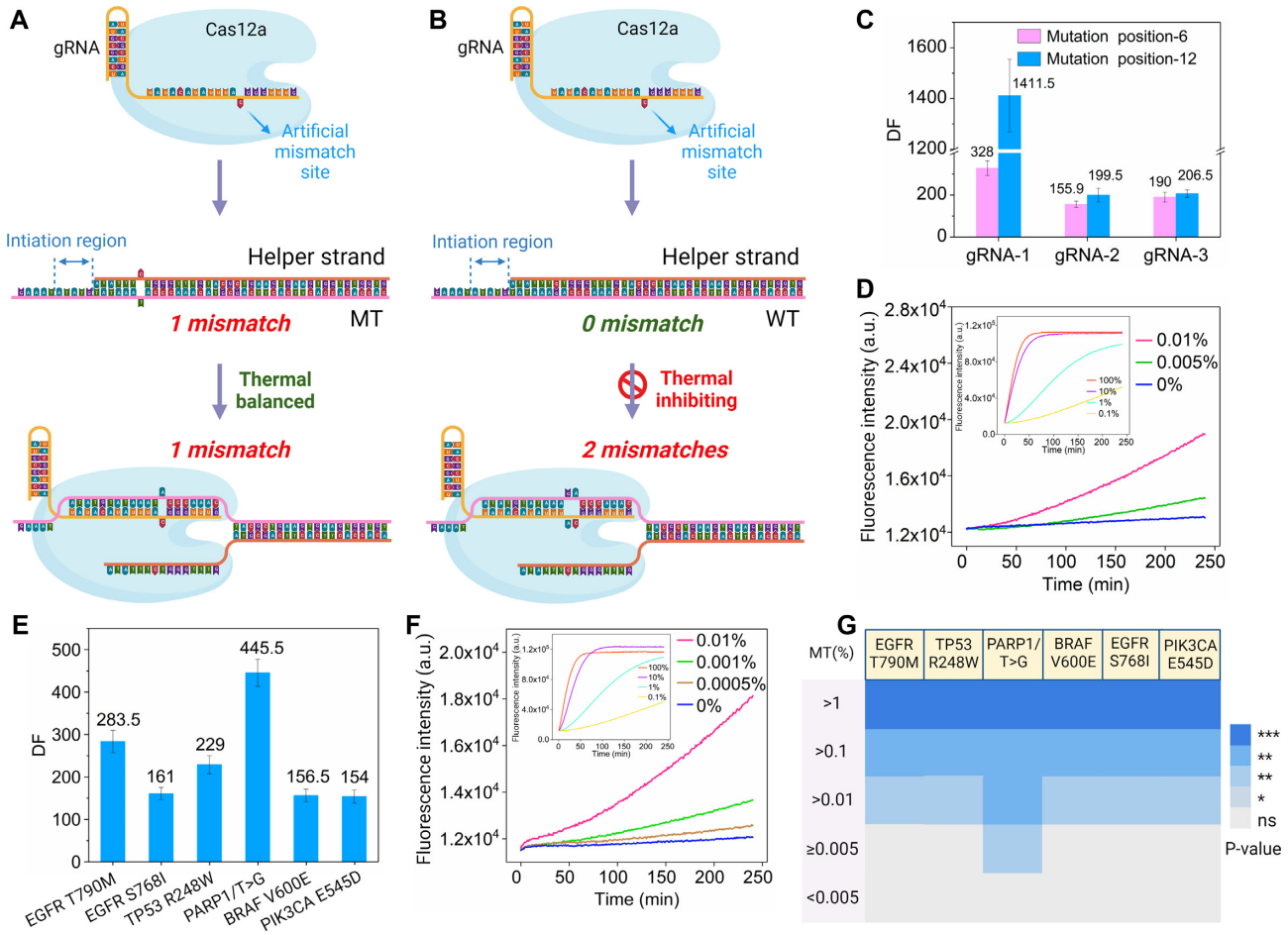

Figure 4. (**A**) and (**B**) Schematic illustration of improving the detection performance of CRISPR-Cas12a toward low-abundance point mutations by introducing a Helper strand and incorporating an artificial mismatch site into gRNA; the Helper strand was designed to be complementary to WT and single-base mismatched with MT. (**C**) The DFs of the CRISPR-Cas12a system toward MT and WT when gRNA-1, gRNA-2 and gRNA-3 were used and the mismatch to be detected was located at position 6 or 12. Reaction setup: 100 nM B-strand, 500 nM Helper strand, 20 nM LbaCas12a, 10 nM gRNA and 200 nM ssDNA FQ probe. (**D**) The detection limit for low-abundance synthesized targeting strand. gRNA-1 was used and the mismatch site to be detected was at position 12. Reaction setup: 200 nM targeting strand, 1000 nM Helper strand, 20 nM LbaCas12a, 10 nM gRNA and 200 nM ssDNA FQ probe. (**E**) The DFs of the CRISPR-Cas12a system toward six point mutations with clinical significance: EGFR T790M, EGFR S768I, TP53 R248W, PARP1, BRAF V600E and PIK3CA E545D. Reaction setup: 100 nM substrate DNA, 500 nM Helper strand, 20 nM LbaCas12a, 10 nM gRNA and 200 nM ssDNA FQ probe. (**F**) The detection limit for low-abundance synthesized MT strand of PARP1. Reaction setup: 200 nM substrate DNA, 1000 nM Helper strand, 20 nM LbaCas12a, 10 nM gRNA and 200 nM ssDNA FQ probe (labeled with FAM and BHQ-1). (**G**) Statistical analysis of the detection limits of CRISPR-Cas12a toward low-abundance synthesized MT strands of EGFR T790M, TP53 R248W PARP1, BRAF V600E, EGFR S768I and PIK3CA E545D. All of the experiments were conducted in triplicate. Results are demonstrated as the mean ± SD. Student's *t*-test, ns, $P > 0.05$; *$P < 0.05$; **$P < 0.01$; ***$P < 0.001$.

and Helper strand were heated to 95°C for 10 min, annealed to 37°C for 10 min, added with CRISPR-Cas12a and probe and immediately underwent fluorescence measurement. For workflow 3, the PCR products and Helper strand were heated to 95°C for 10 min, annealed to 0°C for 5 min, added with CRISPR-Cas12a and incubated for 1 min, then the probe was added and immediately underwent fluorescence measurement at 37°C. Experimental results in Figure 5D and E show that the signal of mutant-type and wild-type plasmids were both very weak when using workflow 2. Compared with workflow 1, we could conclude that the unique DNA hybridization kinetics at low temperature were critical for the CRISPR-Cas12a system to function on genomic DNA. Also, when using workflow 3, the signal induced by mutant-type plasmid was strong, and the DF was also very high (157). However, the reaction rate of mutant-type plasmid became slower, i.e. only 60% of the rate when using workflow 1. Such a decrease of the reaction rate was due to the less incubation time of CRISPR-Cas12a with its substrate DNAs at 0°C, demonstrating that CRISPR-Cas12a was able to recognize $PAM^{-}SE^{+}$ dsDNA at low temperature, and its ultra-high specificity remained under such a temperature. Overall, we could conclude the mechanism of our established workflow: the *trans*-cleavage activity of the CRIPSR-Cas12a system could be activated specifically by the MT/Helper duplex at 0°C. When recovered to 37°C, although the Helper strand could be displaced by the non-targeted strand of PCR products, the cleavage of probes had already started and would not be affected. We then utilized the above-established workflow to detect

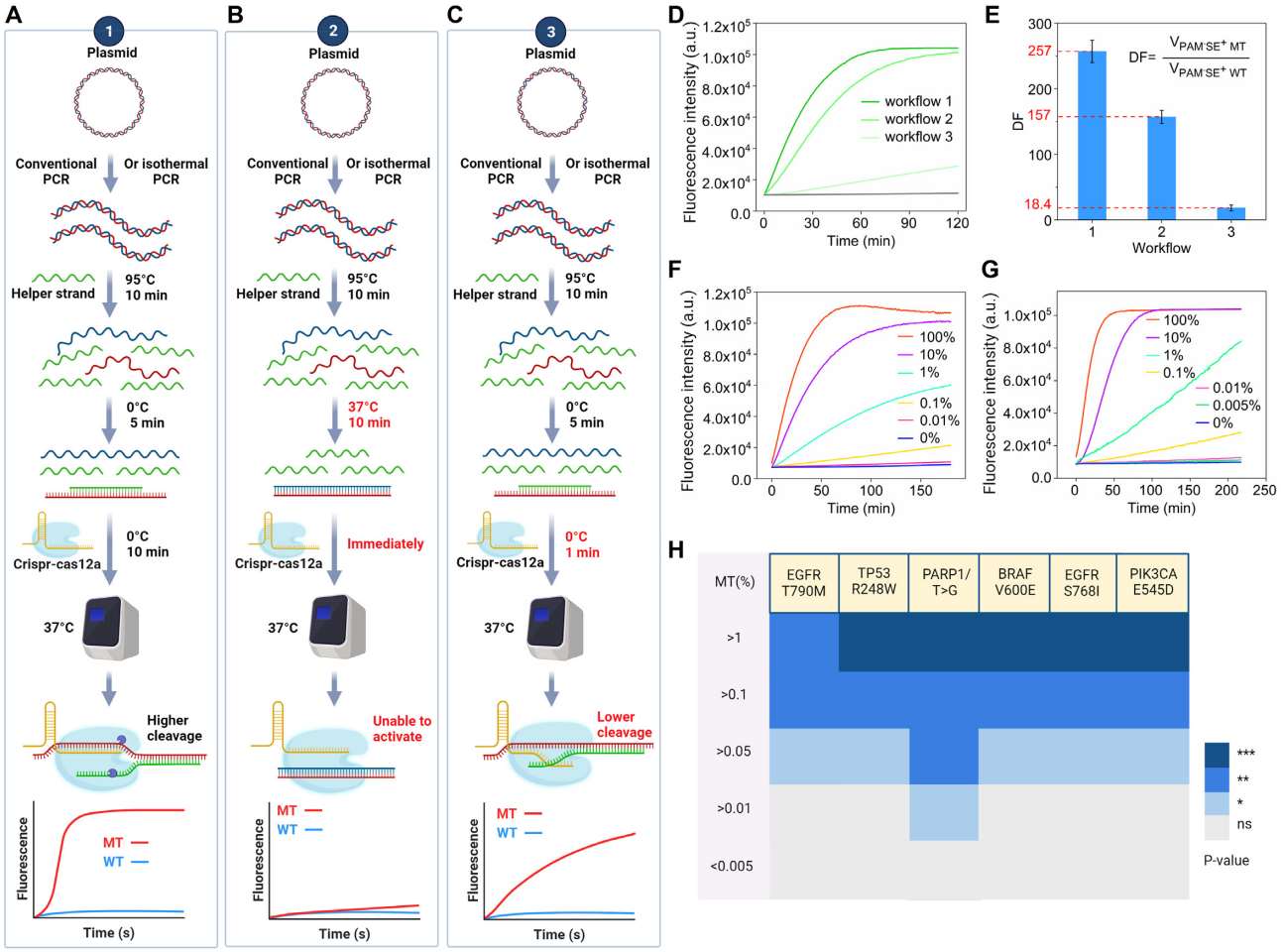

Figure 5. (**A**–**C**) Schematic illustration of the workflows for combining PCR amplification with the CRISPR-Cas12a system. The strategies for transformation of dsDNA product to ssDNA in workflows 1, 2 and 3 are different. Specifically, in workflows 1 and 3, we observed the low-temperature activation phenomenon of CRISPR-Cas12a. (**D**) The cleavage efficiency of CRISPR-Cas12a activated by the PCR products of MT and WT plasmids of EGFR T790M following different workflows. Reaction setup: 10 ng of plasmid DNA, 4000 nM Helper strand, 40 nM LbaCas12a, 20 nM gRNA and 200 nM ssDNA FQ probe. (**E**) The DFs of CRISPR-Cas12a toward MT and WT plasmids of EGFR T790M following different workflows. (**F**) and (**G**) The detection limits for low-abundance targeting MT plasmids of EGFR T790M and PARP1 following workflow 1. Reaction setup: 10 ng of plasmid DNA, 4000 nM Helper strand, 40 nM LbaCas12a, 20 nM gRNA and 200 nM ssDNA FQ probe. (**H**) The detection limits of CRISPR-Cas12a toward low-abundance MT plasmid DNA of EGFR T790M, EGFR S768I, TP53 R248W, PARP1, BRAF V600E and PIK3CA E545D. All of the experiments were repeated three times. Results are shown as the mean ± SD. Student's *t*-test, ns, $P > 0.05$; *$P < 0.05$; **$P < 0.01$; ***$P < 0.001$.

low-abundance point mutations with clinical significance in plasmid samples. We synthesized mutant-type and wild-type plasmids and primers of other mutations (DNA sequences are given in Supplementary Table S6). As shown in Figure 5F and G and Supplementary Figure S5a–d, the detection limits were 0.01–0.05% toward the six tested targeting mutations, demonstrating the functionality of our established system on genomic samples.

We would also like to discuss the advantages and disadvantages of our proposed workflow. We admit that after PCR, we still need to conduct a treatment for controlling increases and decreases in temperature. However, if such control is coupled to prior normal PCR which is already a process of drastic variation of temperature, we believe that performing one more cycle of temperature variation in the same PCR instrument would be quite convenient. Nevertheless, for some situations where it is very difficult to obtain ice (0°C) or where a prior isothermal PCR was used and users wish to keep the temperature unchanged, our post-PCR treatment would then be a little user-unfriendly. In such cases, we suggest that users adopt two other common methods for producing single-stranded substrates: lambda exonucleases digestion (45) and asymmetric PCR (46). However, we would like to note that using those two strategies, many additional reactants are introduced into the system, which requires the users to carefully optimize the reaction set-ups, and the system's functionality might not be stable to different sequences.

Compatibility of the mutation detection system with the gold nanoparticle-based FRET system

To further enhance the application potential of our system, we tested its compatibility with other signal transduction methods, such as the AuNP-based fluorescence resonance energy transfer (FRET) system. As we know,

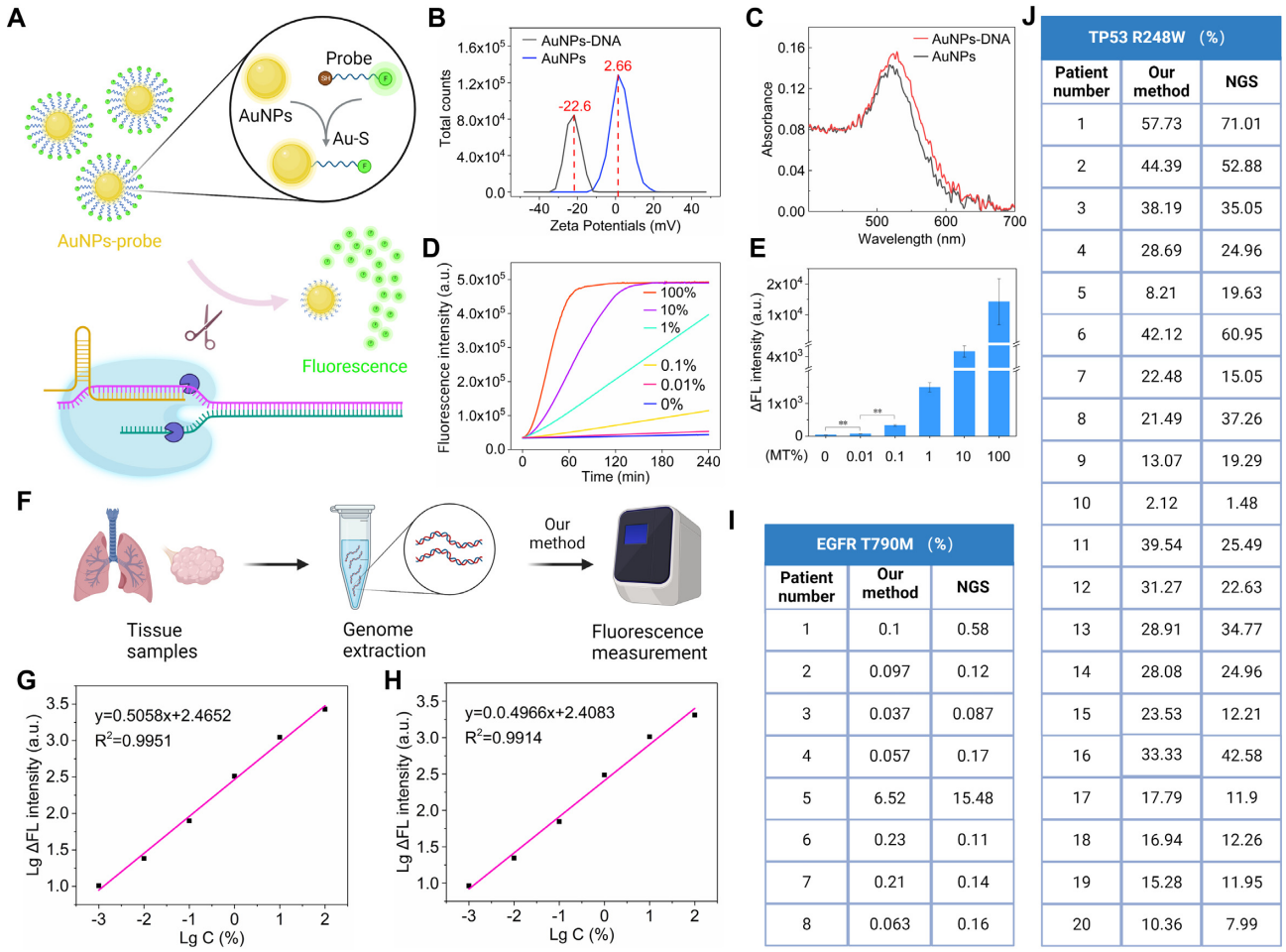

I

EGFR T790M (%)		
Patient number	Our method	NGS
1	0.1	0.58
2	0.097	0.12
3	0.037	0.087
4	0.057	0.17
5	6.52	15.48
6	0.23	0.11
7	0.21	0.14
8	0.063	0.16

J

TP53 R248W (%)		
Patient number	Our method	NGS
1	57.73	71.01
2	44.39	52.88
3	38.19	35.05
4	28.69	24.96
5	8.21	19.63
6	42.12	60.95
7	22.48	15.05
8	21.49	37.26
9	13.07	19.29
10	2.12	1.48
11	39.54	25.49
12	31.27	22.63
13	28.91	34.77
14	28.08	24.96
15	23.53	12.21
16	33.33	42.58
17	17.79	11.9
18	16.94	12.26
19	15.28	11.95
20	10.36	7.99

Figure 6. (**A**) Schematic illustration of the synthesis of AuNP–DNA probes and the process of CRISPR-Cas12a cleaving the AuNP–DNA probes. The ratio of AuNPs to DNA is 1:2000. (**B**) UV-vis absorbance spectrum of the AuNP–DNA probes. (**C**) The zeta potential value of the AuNP–DNA probes. (**D**) and (**E**) The detection limits for low-abundance MT plasmid DNA of EGFR T790M by AuNP–DNA probes. Reaction setup: 10 ng of plasmid DNA, 4000 nM Helper strand, 40 nM LbaCas12a, 20 nM gRNA and 0.2 nM AuNP–DNA probe. All of the experiments were conducted in triplicate. Results are shown as the mean ± SD. Student's *t*-test, ns, $P > 0.05$; $^{*}P < 0.05$; $^{**}P < 0.01$; $^{***}P < 0.001$. (**F**) Schematic workflow for mutation detection in real clinical samples by our method. (**G**) and (**H**) The standard curves of detection of low-abundance EGFR T790M and TP53 R248W mutations. Lg C, the logarithm of target concentration. Lg ΔFL intensity, the logarithm of the increasing rate of the fluorescence intensity. (**I**) Comparison of the abundances of the EGFR T790M mutation in eight clinical samples reported by our method and next-generation sequencing (NGS). (**J**) Comparison of the abundances of the TP53 R248W mutation in 20 clinical samples reported by our method and NGS.

AuNPs are able to quench a variety of fluorophores including FAM, Cy-3 and Cy-5 (47). Therefore, it would be an ideal quencher for multiplexed detection, which is indeed needed for molecular diagnosis of cancer because carcinogenesis is often induced by multiple mutations. As shown in Figure 6A, the single-strand signal probe was labeled with a FAM, and its opposite end was labeled with a sulfhydryl group (Probe-2). The signal probes aggregated on the AuNPs because of the formation of Au–S bonds, and the signal–probe-modified AuNPs served as the signal transduction module. The initial fluorescence was quenched by the AuNPs, and when the CRISPR-Cas12a was activated by targeting substrates, it would cleave the signal probes on the surface of the nanoparticles. Consequently, the FAM-labeled fragment left the nanoparticle and emitted a fluorescent signal. First, we confirmed the successful synthesis of the AuNP–DNA probe by its UV-vis absorbance spectrum (Figure 6B), zeta potential values (Figure 6C) and TEM (Supplementary Figure S6a). Then, we applied the AuNP-based CRISPR-Cas12a system to discriminate the single-base mismatches and detect low-abundance point mutations in the synthesized strands and plasmid genomic DNA of EGFR T790M. As shown in Figures 6D and E and Supplementary Figure S6b and c, the detection limits were 0.005% for synthesized strands and 0.01% for plasmid genomic DNA, demonstrating that our proposed CRISPR-Cas12a system was compatible with the AuNP-based FRET system and thereby shows great potential in further development of multiplexed assays.

Application of the proposed detection system to clinical samples

Finally, we applied our method to the analysis of real clinical samples. Taking the ovarian cancer-related TP53 R248W and lung cancer-related EGFR T790M mutations

as our targets, we collected 20 tissue samples from ovarian cancer patients and 8 tissue samples from lung cancer patients. The genomic DNAs extracted from the above samples were first analyzed by NGS and verified to contain the TP53 R248W mutation or the EGFR T790M mutation. Thereafter, we used our proposed CRISPR-Cas12a system to analyze the samples following the workflow depicted in Figure 6F. To calculate the true abundances of TP53 R248W or EGFR T790M mutations in the tested samples, we conducted detection tests on the plasmid genomic DNA samples with several known mutation abundances and plotted the standard curves (Figure 6G, H). Thereafter, we calculated the mutation abundances of the clinical samples. As shown in Figure 6I and J, and Supplementary Figures S7 and S8, the mutation abundances provided by our method ranged from 0.037% to 57.73% and, more importantly, our results were in very good agreement with the NGS results, with an average deviation of 6.146%. The excellent performance of our method on real clinical samples firmly demonstrates its clinical practicability. It is worth noting that the assays for low-abundance mutation detection could be mainly classified into four categories: sequencing based, ddPCR based, real-time PCR based and post-PCR probe based. The former two categories rely on expensive instruments, and real-time PCR-based methods are less sensitive. Post-PCR probe-based assays inherit the advantages of convenience and low cost of normal PCR, and moreover they are compatible with target recognition and signal amplification by various nuclease, such as Flap endonuclease (48) and endonuclease IV (49). As we have discussed in the Introduction, Cas12a is unique and distinct compared with those commonly used nucleases due to its ultra-powerful signal amplification efficiency. Therefore, after unraveling the bottleneck restraint of poor specificity and limited generality of Cas12a, we unleashed the great potential of the CRISPR-Cas12a system in the detection of low-abundance point mutations. In comparison with other post-PCR probe-based assays, our method's sensitivity is among the highest and the sequence design is simpler and more robust to different targets. We would also like to point out that the biggest problem or disadvantage of our method is the relatively cumbersome post-PCR treatment. Just like other post-PCR probe-based assays, the substrate for probe analysis is ssDNA and thereby post-PCR treatment to produce single-stranded substrate is inevitable. Here, in our work, we have endeavored to simplify the process by taking advantages of the low-temperature activation property of Cas12a. We do not need to add any additional reactants or introduce any separation steps, but we still need to adjust the temperature up and down, which could be user-unfriendly in some cases. Overall, the main drawback of the post-PCR probe-based assays including the established method herein is the inconvenience and workload of post-PCR treatment, but this may be solved by further investigations on the reactions between nucleases and nucleic acids.

CONCLUSION

To sum up, we have discovered a novel substrate DNA for CRISPR-Cas12a, namely $PAM^{-}SE^{+}$ dsDNA, and revealed that CRISPR-Cas12a possessed two unique properties toward this novel substrate: (i) the ability to recognize and cleave dsDNA without requiring a PAM sequence and (ii) its ultra-sensitivity toward mismatches within the substrate dsDNA, with DFs ranging from 8.2 to 11.3 (median 8.6), which is nearly 4-fold higher than conventional substrates. Further mechanism studies revealed that gRNA formed a triple-stranded flap structure with the substrate dsDNA that could guide CRISPR-Cas12a to cleave dsDNA at both strands without a PAM sequence, and was significantly more sensitive to slight sequence changes. Based on the novel targeting properties of CRISPR-Cas12a, we introduced a Helper strand that further enhanced the DF to between 155 and 1411 (median 207), and the detection limits for low-abundance point mutations were greatly decreased to 0.0005–0.01%. In addition, we discovered the property of low-temperature activation of CRISPR-Cas12a, and constructed a complete workflow for low-abundance point mutation detection in real samples by coupling unique DNA hybridization kinetics at low temperature with the RPA or PCR amplification process. The detection limits were 0.005–0.01% toward synthesized DNA and 0.05–0.01% toward plasmid genomic DNA, and the mutation abundances provided by our system for 28 real clinical samples were in accordance with NGS results.

Collectively, we have discovered a brand new targeting substrate for CRISPR-Cas12a and, toward this substrate, the sensitivity, specificity and generality of the CRISPR-Cas12a system have reached unity. A further revealed property of low-temperature activation allowed the CRISPR-Cas12a system to easily combine DNA amplification technologies, which ultimately achieved fast, convenient, accurate and sensitive detection of low-abundance point mutations. We firmly believe our work not only significantly deepened our understanding of the CRISPR-Cas12a system, but also greatly broadened its application scenarios.

DATA AVAILABILITY

Supplementary data are available at NAR online. Other relevant data are available from the authors upon reasonable request.

SUPPLEMENTARY DATA

Supplementary Data are available at NAR Online.

ACKNOWLEDGEMENTS

Author contributions: Z.W. and M.Y.Q. designed the overall research strategy, and coordinated data collection and manuscript writing. X.X.J., W.H.B. and L.L.J. were the lead researchers for conceptualization of the project, data analysis and manuscript writing. D.K.J., Z.L., Y.B., H.H., L.Y.W., Z.R., S.W. and Y.Z.X. participated in the related experiments. L.Y.P., W.C. and S.Q.Q. collected clinical samples and extracted tissue DNA. All authors were involved in the preparation of the final manuscript.

FUNDING

This work was financially supported by the National Key Research and Development Program of China

[2021YFC2701402]; National Natural Science Foundation of China [81871732]; the Open Research Fund of State Key Laboratory of Bioelectronics, South-east University [Sklb2021-k06]; Open Project Fund from NHC Key Lab of Reproduction Regulation [KF2021-02]; the Open Research Fund of State Key Laboratory of Advanced Technology for Materials Synthesis and Processing (Wuhan University of Technology) [2022-KF-2]; and the Huazhong University of Science and Technology Innovation Research Institute Science and Technology Innovation Fund [2022JYCXJJ045]. Funding for open access charge: Insititute of Reproductive Health, Tongji Medical College, Huazhong University of Science and Technology.

Conflict of interest statement. Huazhong University of Science and Technology has filed a provisional patent on the described technologies and there are no other competing financial interests.

REFERENCES

1. Jinek,M., Chylinski,K., Fonfara,I., Hauer,M., Doudna,J.A. and Charpentier,E. (2012) A programmable dual-RNA-guided DNA endonuclease in adaptive bacterial immunity. *Science*, **337**, 816–821.
2. Pickar-Oliver,A. and Gersbach,C.A. (2019) The next generation of CRISPR-Cas technologies and applications. *Nat. Rev. Mol. Cell Biol.*, **20**, 490–507.
3. Hendriks,D., Clevers,H. and Artegiani,B. (2020) CRISPR-Cas tools and their application in genetic engineering of human stem cells and organoids. *Cell Stem. Cell*, **27**, 705–731.
4. Sander,J.D. and Joung,J.K. (2014) CRISPR-Cas systems for editing, regulating and targeting genomes. *Nat. Biotechnol.*, **32**, 347–355.
5. Yan,W.X., Hunnewell,P., Alfonse,L.E., Carte,J.M., Keston-Smith,E., Sothiselvam,S., Garrity,A.J., Chong,S., Makarova,K.S., Koonin,E.V. *et al.* (2019) Functionally diverse type v CRISPR-Cas systems. *Science*, **363**, 88–91.
6. Jinek,M., Chylinski,K., Fonfara,I., Hauer,M., Doudna,J.A. and Charpentier,E. (2012) A programmable dual-RNA-guided DNA endonuclease in adaptive bacterial immunity. *Science*, **337**, 816–821.
7. Mali,P., Yang,L., Esvelt,K.M., Aach,J., Guell,M., DiCarlo,J.E., Norville,J.E. and Church,G.M. (2013) RNA-guided human genome engineering via cas9. *Science*, **339**, 823–826.
8. Zetsche,B., Gootenberg,J.S., Abudayyeh,O.O., Slaymaker,I.M., Makarova,K.S., Essletzbichler,P., Volz,S.E., Joung,J., van der Oost,J., Regev,A. *et al.* (2015) Cpf1 is a single RNA-guided endonuclease of a class 2 CRISPR-Cas system. *Cell*, **163**, 759–771.
9. Li,S.Y., Cheng,Q.X., Liu,J.K., Nie,X.Q., Zhao,G.P. and Wang,J. (2018) CRISPR-Cas12a has both cis- and trans-cleavage activities on single-stranded DNA. *Cell Res.*, **28**, 491–493.
10. Chen,J.S., Ma,E., Harrington,L.B., Da,C.M., Tian,X., Palefsky,J.M. and Doudna,J.A. (2018) CRISPR-Cas12a target binding unleashes indiscriminate single-stranded DNase activity. *Science*, **360**, 436–439.
11. Li,S.Y., Cheng,Q.X., Wang,J.M., Li,X.Y., Zhang,Z.L., Gao,S., Cao,R.B., Zhao,G.P. and Wang,J. (2018) CRISPR-Cas12a-assisted nucleic acid detection. *Cell. Discov.*, **4**, 20.
12. Gootenberg,J.S., Abudayyeh,O.O., Kellner,M.J., Joung,J., Collins,J.J. and Zhang,F. (2018) Multiplexed and portable nucleic acid detection platform with cas13, cas12a, and csm6. *Science*, **360**, 439–444.
13. Xiong,Y., Zhang,J., Yang,Z., Mou,Q., Ma,Y., Xiong,Y. and Lu,Y. (2020) Functional DNA regulated CRISPR-Cas12a sensors for point-of-care diagnostics of non-nucleic-acid targets. *J. Am Chem. Soc.*, **142**, 207–213.
14. Liang,M., Li,Z., Wang,W., Liu,J., Liu,L., Zhu,G., Karthik,L., Wang,M., Wang,K.F., Wang,Z. *et al.* (2019) A CRISPR-Cas12a-derived biosensing platform for the highly sensitive detection of diverse small molecules. *Nat. Commun.*, **10**, 3672.
15. Chen,X., Liu,N., Liu,L., Chen,W., Chen,N., Lin,M., Xu,J., Zhou,X., Wang,H., Zhao,M. *et al.* (2019) Thermodynamics and kinetics guided probe design for uniformly sensitive and specific DNA hybridization without optimization. *Nat. Commun.*, **10**, 4675.
16. Wu,T., Chen,W., Yang,Z., Tan,H., Wang,J., Xiao,X., Li,M. and Zhao,M. (2018) DNA terminal structure-mediated enzymatic reaction for ultra-sensitive discrimination of single nucleotide variations in circulating cell-free DNA. *Nucleic Acids Res.*, **46**, e24.
17. Xiao,X., Wu,T., Xu,L., Chen,W. and Zhao,M. (2017) A branch-migration based fluorescent probe for straightforward, sensitive and specific discrimination of DNA mutations. *Nucleic Acids Res.*, **45**, e90.
18. Zuo,X., Xia,F., Xiao,Y. and Plaxco,K.W. (2010) Sensitive and selective amplified fluorescence DNA detection based on exonuclease III-aided target recycling. *J. Am Chem. Soc.*, **132**, 1816–1818.
19. Shi,K., Xie,S., Tian,R., Wang,S., Lu,Q., Gao,D., Lei,C., Zhu,H. and Nie,Z. (2021) A CRISPR-Cas autocatalysis-driven feedback amplification network for supersensitive DNA diagnostics. *Sci. Adv.*, **7**, eabc7802.
20. Kim,D., Luk,K., Wolfe,S.A. and Kim,J.S. (2019) Evaluating and enhancing target specificity of gene-editing nucleases and deaminases. *Annu. Rev. Biochem.*, **88**, 191–220.
21. Strohkendl,I., Saifuddin,F.A., Rybarski,J.R., Finkelstein,I.J. and Russell,R. (2018) Kinetic basis for DNA target specificity of CRISPR-Cas12a. *Mol. Cell*, **71**, 816–824.
22. Dou,Y., Gold,H.D., Luquette,L.J. and Park,P.J. (2018) Detecting somatic mutations in normal cells. *Trends Genet.*, **34**, 545–557.
23. Li,X., Ye,M., Zhang,W., Tan,D., Jaffrezic-Renault,N., Yang,X. and Guo,Z. (2019) Liquid biopsy of circulating tumor DNA and biosensor applications. *Biosens. Bioelectron.*, **126**, 596–607.
24. Leong,K.W., Yu,F. and Makrigiorgos,G.M. (2022) Mutation enrichment in human DNA samples via UV-mediated cross-linking. *Nucleic Acids Res.*, **50**, e32.
25. Marino,N.D., Pinilla-Redondo,R. and Bondy-Denomy,J. (2022) CRISPR-Cas12a targeting of ssDNA plays no detectable role in immunity. *Nucleic Acids Res.*, **50**, 6414–6422.
26. Kim,H., Lee,S., Yoon,J., Song,J. and Park,H.G. (2021) CRISPR/Cas12a collateral cleavage activity for simple and rapid detection of protein/small molecule interaction. *Biosens. Bioelectron.*, **194**, 113587.
27. Kim,H., Lee,W.J., Oh,Y., Kang,S.H., Hur,J.K., Lee,H., Song,W., Lim,K.S., Park,Y.H., Song,B.S. *et al.* (2020) Enhancement of target specificity of CRISPR-Cas12a by using a chimeric DNA–RNA guide. *Nucleic Acids Res.*, **48**, 8601–8616.
28. Ke,Y., Ghalandari,B., Huang,S., Li,S., Huang,C., Zhi,X., Cui,D. and Ding,X. (2022) 2′-O-Methyl modified guide RNA promotes the single nucleotide polymorphism (SNP) discrimination ability of CRISPR-Cas12a systems. *Chem. Sci.*, **13**, 2050–2061.
29. Smith,S.J., Nemr,C.R. and Kelley,S.O. (2017) Chemistry-driven approaches for ultrasensitive nucleic acid detection. *J. Am Chem. Soc.*, **139**, 1020–1028.
30. Kaminski,M.M., Abudayyeh,O.O., Gootenberg,J.S., Zhang,F. and Collins,J.J. (2021) CRISPR-based diagnostics. *Nat. Biomed. Eng.*, **5**, 643–656.
31. Chen,Y., Mei,Y. and Jiang,X. (2021) Universal and high-fidelity DNA single nucleotide polymorphism detection based on a CRISPR/Cas12a biochip. *Chem. Sci.*, **12**, 4455–4462.
32. Ooi,K.H., Liu,M.M., Tay,J., Teo,S.Y., Kaewsapsak,P., Jin,S., Lee,C.K., Hou,J., Maurer-Stroh,S., Lin,W. *et al.* (2021) An engineered CRISPR-Cas12a variant and DNA–RNA hybrid guides enable robust and rapid COVID-19 testing. *Nat. Commun.*, **12**, 1739.
33. Zetsche,B., Gootenberg,J.S., Abudayyeh,O.O., Slaymaker,I.M., Makarova,K.S., Essletzbichler,P., Volz,S.E., Joung,J., van der Oost,J., Regev,A. *et al.* (2015) Cpf1 is a single RNA-guided endonuclease of a class 2 CRISPR-Cas system. *Cell*, **163**, 759–771.
34. Li,H., Cui,X., Sun,L., Deng,X., Liu,S., Zou,X., Li,B., Wang,C., Wang,Y., Liu,Y. *et al.* (2021) High concentration of cas12a effector tolerates more mismatches on ssDNA. *FASEB J.*, **35**, e21153.
35. Wang,J.S. and Zhang,D.Y. (2015) Simulation-guided DNA probe design for consistently ultraspecific hybridization. *Nat. Chem.*, **7**, 545–553.
36. Cohen,J.D., Li,L., Wang,Y., Thoburn,C., Afsari,B., Danilova,L., Douville,C., Javed,A.A., Wong,F., Mattox,A. *et al.* (2018) Detection and localization of surgically resectable cancers with a multi-analyte blood test. *Science*, **359**, 926–930.
37. Loeb,L.A. (2011) Human cancers express mutator phenotypes: origin, consequences and targeting. *Nat. Rev. Cancer*, **11**, 450–457.

38. Joshi,S.K., Qian,K., Bisson,W.H., Watanabe-Smith,K., Huang,A., Bottomly,D., Traer,E., Tyner,J.W., McWeeney,S.K., Davare,M.A. *et al.* (2020) Discovery and characterization of targetable NTRK point mutations in hematologic neoplasms. *Blood*, **135**, 219–2170.
39. Martincorena,I. and Campbell,P.J. (2015) Somatic mutation in cancer and normal cells. *Science*, **349**, 1483–1489.
40. Chang,M.T., Asthana,S., Gao,S.P., Lee,B.H., Chapman,J.S., Kandoth,C., Gao,J., Socci,N.D., Solit,D.B., Olshen,A.B. *et al.* (2016) Identifying recurrent mutations in cancer reveals widespread lineage diversity and mutational specificity. *Nat. Biotechnol.*, **34**, 155–163.
41. Han,K., Lee,T.Y., Nikitopoulos,D.E., Soper,S.A. and Murphy,M.C. (2011) A vertically stacked, polymer, microfluidic point mutation analyzer: rapid high accuracy detection of low-abundance K-ras mutations. *Anal. Biochem.*, **417**, 211–219.
42. Shah,S.P., Morin,R.D., Khattra,J., Prentice,L., Pugh,T., Burleigh,A., Delaney,A., Gelmon,K., Guliany,R., Senz,J. *et al.* (2009) Mutational evolution in a lobular breast tumour profiled at single nucleotide resolution. *Nature*, **461**, 809–813.
43. Haworth,S., Shapland,C.Y., Hayward,C., Prins,B.P., Felix,J.F., Medina-Gomez,C., Rivadeneira,F., Wang,C., Ahluwalia,T.S., Vrijheid,M. *et al.* (2019) Low-frequency variation in TP53 has large effects on head circumference and intracranial volume. *Nat. Commun.*, **10**, 357.
44. Chen,S., Wang,R., Peng,S., Xie,S., Lei,C., Huang,Y. and Nie,Z. (2022) PAM-less conditional DNA substrates leverage trans-cleavage of CRISPR-Cas12a for versatile live-cell biosensing. *Chem. Sci.*, **13**, 2011–2020.
45. Chen,X., Liu,N., Liu,L., Chen,W., Chen,N., Lin,M., Xu,J., Zhou,X., Wang,H.B., Zhao,M.P. *et al.* (2019) Thermodynamics and kinetics guided probe design for uniformly sensitive and specific DNA hybridization without optimization. *Nat. Commun.*, **10**, 4675.
46. Sanchez,J.A., Pierce,K.E., Rice,J.E. and Wangh,L.J. (2004) Linear-after-the-exponential (LATE)-PCR: an advanced method of asymmetric PCR and its uses in quantitative real-time analysis. *Proc. Natl Acad. Sci. USA*, **101**, 1933–1938.
47. Kan,A., Wang,S., Zhang,L., Xu,X., Zhang,N. and Jiang,W. (2021) A functional DNA-modified dual-response gold nanoprobe for simultaneously imaging the acidic microenvironment and membrane proteins of tumor cells. *Talanta*. **229**, 122284.
48. Cheng,X., Bao,Y., Liang,S., Li,B., Liu,Y., Wu,H., Ma,X., Chu,Y., Shao,Y., Meng,Q. *et al.* (2021) Flap endonuclease 1-assisted DNA walkers for sensitively and specifically sensing ctDNAs. *Anal. Chem.*, **93**, 9593–9601.
49. Zhang,W., Liu,L., Liao,Y., Shu,W., Tang,X., Dong,K., Ming,Z., Xiao,X. and Wang,H. (2022) Thermodynamics-guided two-way interlocking DNA cascade system for universal multiplexed mutation detection. *Chin. Chem. Lett.*, **33**, 334–338.